JACS
JOURNAL OF THE AMERICAN CHEMICAL SOCIETY
pubs.acs.org/JACS
Article

Central Core-Twisted Conformation Acceptors Achieving 20.60% Efficiency via Suppression of Nonradiative Losses without Sacrificing Current and Fill Factor in Binary Organic Solar Cells

Ruohan Wang,[‡] Xiaodong Si,[‡] Le Mei, Wenkai Zhao, Wendi Shi, Xian-Kai Chen,* Guangkun Song, Longyu Li, Zheng Xiao, Zhaoyang Yao, Guankui Long, Chenxi Li, Xiangjian Wan,* and Yongsheng Chen*

Cite This: J. Am. Chem. Soc. 2025, 147, 43629−43639

Read Online

ACCESS | Metrics & More | Article Recommendations | Supporting Information

ABSTRACT: Designing acceptors with low nonradiative energy losses without compromising short-circuit current density and fill factor remains a critical challenge for achieving high-efficiency organic solar cells. In this study, we design and synthesize two acceptors, named a-Th2Cl and a-Th2Br, featuring a halogenated thiophene unit grafted via a single bond onto the central core, an approach that extends beyond conventional central core conjugation extension acceptor design. The rotation around the single bond can result in twist conformation, and the aggregation-caused quenching effect during the transition from solution to film is effectively suppressed, favoring increasing photoluminescence quantum yields. X-ray crystal structure analysis reveals that a-Th2Br exhibits unusual molecular packing behavior with strong *J*-aggregation. Theoretical simulation demonstrates that a-Th2Br aggregates exhibit a reduced extent of excited-state charge transfer and enhanced fluorescent oscillator strength compared to the benchmark acceptor L8-BO, rationalizing the observed high photoluminescence quantum yields and low nonradiative energy losses for the two acceptors films and corresponding organic solar cells. Moreover, when blended with PM6, both acceptors yield favorable bulk heterojunction morphologies. As a result, binary organic solar cells based on PM6:a-Th2Cl and PM6:a-Th2Br deliver power conversion efficiencies of 19.87 and 20.60% (certified 20.05%), with impressively low nonradiative energy losses values of 0.202 and 0.194 eV, respectively. These results highlight the potential of central core engineering in simultaneously suppressing nonradiative losses and maintaining a high short-circuit current density and fill factor in high-performance organic solar cells.

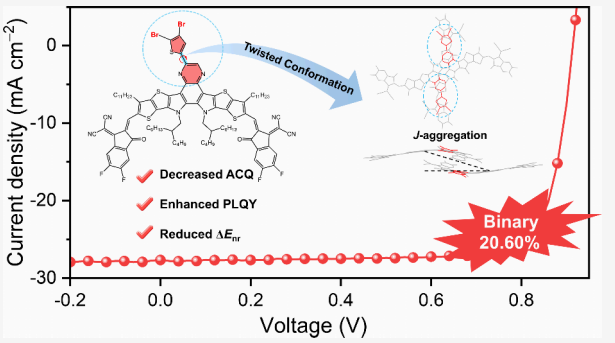

INTRODUCTION

In recent years, significant advancements in organic photovoltaic materials, particularly nonfullerene acceptors, have led to remarkable improvements in the power conversion efficiency (PCE) of organic solar cells (OSCs), with efficiencies now surpassing 20%.[1−9] However, compared to inorganic and perovskite solar cells, OSCs still exhibit relatively lower efficiencies, primarily due to their substantial nonradiative energy losses (ΔE_{nr}) ranging from 0.2 to 0.4 eV,[10−13] resulting in a reduced open-circuit voltage (V_{OC}). Recent studies by Bredas et al. suggest that enhancing the photoluminescence quantum yield (PLQY) of the low-bandgap component in the active layers can reduce ΔE_{nr} in OSCs.[14]

However, low-bandgap fused-ring electron acceptors typically have a longer emission wavelength, at the same time, their almost completely planar configurations can cause severe aggregation-caused quenching (ACQ) effects during aggregation, resulting in very low PLQY in films.[15] To achieve a high PLQY in acceptors, it is crucial to conduct an in-depth analysis of the molecular packing of acceptors. For typical high-performance Y-series acceptors like Y6,[16] BTP-eC9,[17] and L8-BO,[18] single-crystal structural analyses uniformly show that these acceptors have a tendency to form a three-dimensional interpenetrating network structure through strong $\pi-\pi$ interactions. This structure includes *H*-aggregations based on the central core and *J*-aggregations based on the end groups.[19−22] Usually, *H*-aggregates exhibit weak emission or are even nonemissive. This is because in *H*-aggregates, the molecules are arranged in parallel, with strong intermolecular interactions and negative nearest-neighbor coupling, leading to a nonradiative deactivation process.[23−25] Recent work by Bo et

Received: August 2, 2025
Revised: November 2, 2025
Accepted: November 3, 2025
Published: November 10, 2025

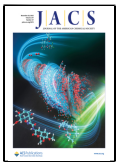

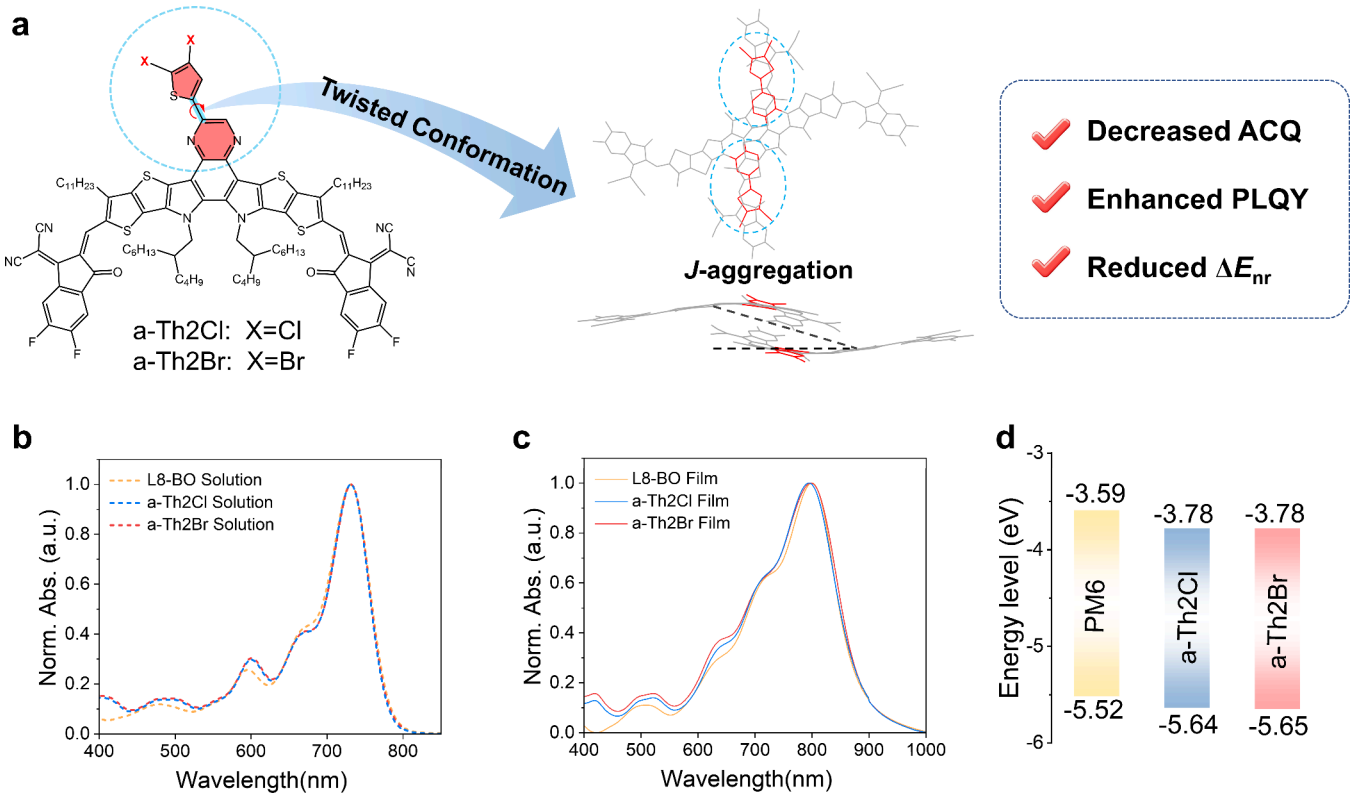

Figure 1. (a) Molecular structures of a-Th2Cl and a-Th2Br. (b, c) Normalized absorption spectra of L8-BO, a-Th2Cl, and a-Th2Br in the $CHCl_3$ solution and in the films. (d) Energy levels of PM6, a-Th2Cl, and a-Th2Br.

al. demonstrated that introducing bulky steric groups to the central core suppresses *H*-aggregation, inhibiting the ACQ effect and yielding significant improvements in PLQY and V_{OC}.[26−28] However, the sharp decline in binary device efficiency serves as a reminder: the complete lack of central participation in stacking may cause excessively severe disruption of molecular packing, which leads to diminished device response and reduced fill factor. For Y-series acceptors, the central core plays a vital role in their photophysical properties, influencing not only absorption, orbital energy levels, and molecular packing, but also crystallinity and charge transport.[15,29−32] Therefore, the modifications of the central core should not completely prevent it from participating in stacking. Instead, the goal is to enable headgroup involvement in stacking while reducing the *H*-aggregate content. This approach strikes a balance between achieving high PLQY, maintaining favorable morphology, and charge carrier mobility, thus enhancing overall device performance. Therefore, it is challenging to design acceptors with suitable intermolecular packing but weak ACQ, which can attribute to obtain high V_{OC} while achieving high J_{SC} and FF.

In this work, we report two acceptors, a-Th2Cl and a-Th2Br (Figure 1a), which feature a central unit with a grafted and halogenated thiophene unit. Notably, compared to the more planar conjugate benchmark acceptor L8-BO (PLQY = 4.40%), they possess the same optical bandgap, but a-Th2Br showed high emission (PLQY = 9.65%). X-ray crystal structure analysis of a-Th2Br demonstrates that the thiophene unit connected via a freely rotatable single bond provides moderate steric hindrance while ensuring central core participation in stacking. This effectively suppressed excessive aggregation.

Meanwhile, a-Th2Br exhibited more obvious *J*-aggregation characteristics while achieving an ordered stacking network, which led to a significant suppression of ACQ (Figure 2e). Compared to L8-BO (ΔE_{nr} = 0.244 eV), devices based on a-Th2Cl and a-Th2Br exhibited significantly reduced ΔE_{nr} of 0.202 and 0.194 eV, respectively, enabling both a-Th2Cl and a-Th2Br systems to achieve V_{OC} over 0.91 V when paired with PM6 as the donor. Consequently, a high PCE of 20.60% (certified 20.05%) was achieved for the PM6:a-Th2Br-based device, with a high V_{OC} of 0.914 V, J_{SC} of 27.67 mA cm^{-2}, and FF of 81.47%. This work demonstrates that the twisted conformation central core can maximize the advantages of Y-series molecular while effectively decoupling the performance limitations of OSCs from high energy losses caused by low luminescence efficiency.

RESULTS AND DISCUSSION

The synthetic route and the corresponding characterization of a-Th2Cl and a-Th2Br are presented in the Supporting Information. The molecular symmetry is expected to directly affect the optoelectronic properties and molecular packing.[33−35] The UV−vis absorptions of a-Th2Cl and a-Th2Br in solution and thin film are shown in Figure 1b. It is worth noting that the absorption edges of the two acceptors are nearly identical to that of L8-BO,[18] a typical Y-series acceptor. This provides an opportunity to directly compare energy losses of their corresponding devices, especially ΔE_{nr}. As depicted in Figure 1b,c, the maximum absorption peaks (λ_{max}) of L8-BO, a-Th2Cl, and a-Th2Br in chloroform are all at 731 nm. In films, the absorptions of L8-BO, a-Th2Cl, and a-Th2Br were all redshifted with λ_{max} peaks at 799, 794, and 799 nm, respectively. This redshift suggests the presence of strong

https://doi.org/10.1021/jacs.5c13302
J. Am. Chem. Soc. 2025, 147, 43629−43639

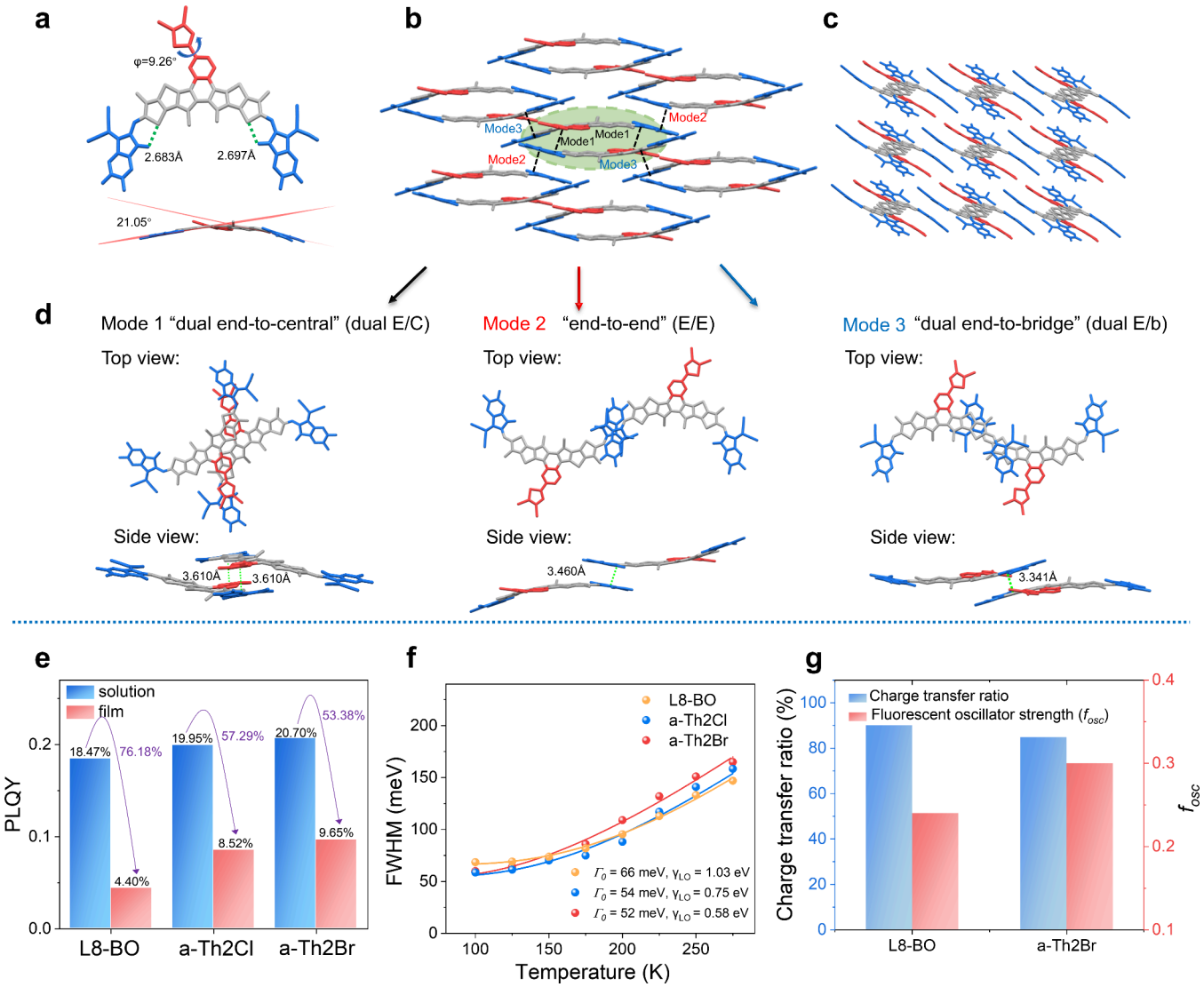

Figure 2. (a) Monomolecular structure of a-Th2Br. (b, c) Molecular packing patterns in a-Th2Br single-crystals. (d) Three types of intermolecular packing modes and corresponding $\pi-\pi$ stacking distances of a-Th2Br. (e) PLQY of a-Th2Cl, a-Th2Br, and L8-BO in solution and film, and corresponding relative values of PLQY decreasing from solution to film. (f) Γ_0 and γ_{LO} calculated from the temperature-dependent PL spectra. (g) The calculated charge-transfer ratio and the fluorescent oscillator strength (f_{osc}) for the S_1 states of L8-BO and a-Th2Br dimers, the values averaged on the 1000 dimers extracted from the MD-simulated films.

intermolecular interactions in the solid films.[36] Figure 1d and Figure S3 present the energy levels of PM6, a-Th2Cl, and a-Th2Br estimated from the cyclic voltammetry (CV) measurement. The HOMO/LUMO energy levels are − 5.64/−3.78 eV for a-Th2Cl and − 5.65/−3.78 eV for a-Th2Br, respectively. The variation of energy levels agrees well with the DFT calculations (Figure S4). To reveal the molecular packing patterns in the solid state, the single crystal of a-Th2Br by the solvent diffusion method has been grown and measured by X-ray diffractions. The corresponding crystallographic data are summarized in Table S12. As shown in Figure 2a, unlike most of Y-series acceptors, a-Th2Br exhibits an unusually nonplanar backbone with a large dihedral angle of 21.05° from the side view. Additionally, the grafted thiophene unit on the central core is also not at the same plane as the adjacent pyrazine unit with a dihedral angle of 9.26°. This special bending structure is conducive to suppress excessive intermolecular aggregation.[37] As displayed in Figure 2d, a-Th2Br possesses three packing modes of "dual end-to-central" (dual E/C), "end-to-end" (E/E), and "dual end-to-bridge" (dual E/b). The corresponding $\pi-\pi$ stacking distances are 3.610 3.460, and 3.341 Å, respectively. Particularly, as shown in Figure 2b, a-Th2Br first forms a dimer stacking through Mode 1 and then each dimer stacks with each other through Mode 2 and Mode 3, thereby forming an ordered two-dimensional (2D) stacking network (Figure 2c), with a molecular packing density (MPD) as high as 61.9%. It is worth noting that all three modes exhibit strong *J*-aggregation properties,[38] which enable the molecule to effectively suppress the aggregation-caused quenching (ACQ) effect and achieve a high PLQY in the aggregated state. The PLQY and time-resolved photoluminescence (TRPL) measurements were carried out to investigate the emission efficiency and exciton lifetime (τ) in two acceptors. As shown in Figure S6, we tested the fluorescence quantum yields of a-Th2Cl, a-Th2Br, and L8-BO in dilute chloroform solutions, which were 19.95, 20.70, and 18.47%, respectively. In thin films, their PLQYs were 8.52, 9.65, and 4.40%, respectively. The relative values of PLQY decreasing from solution to film for L8-BO, a-

https://doi.org/10.1021/jacs.5c13302
J. Am. Chem. Soc. 2025, 147, 43629−43639

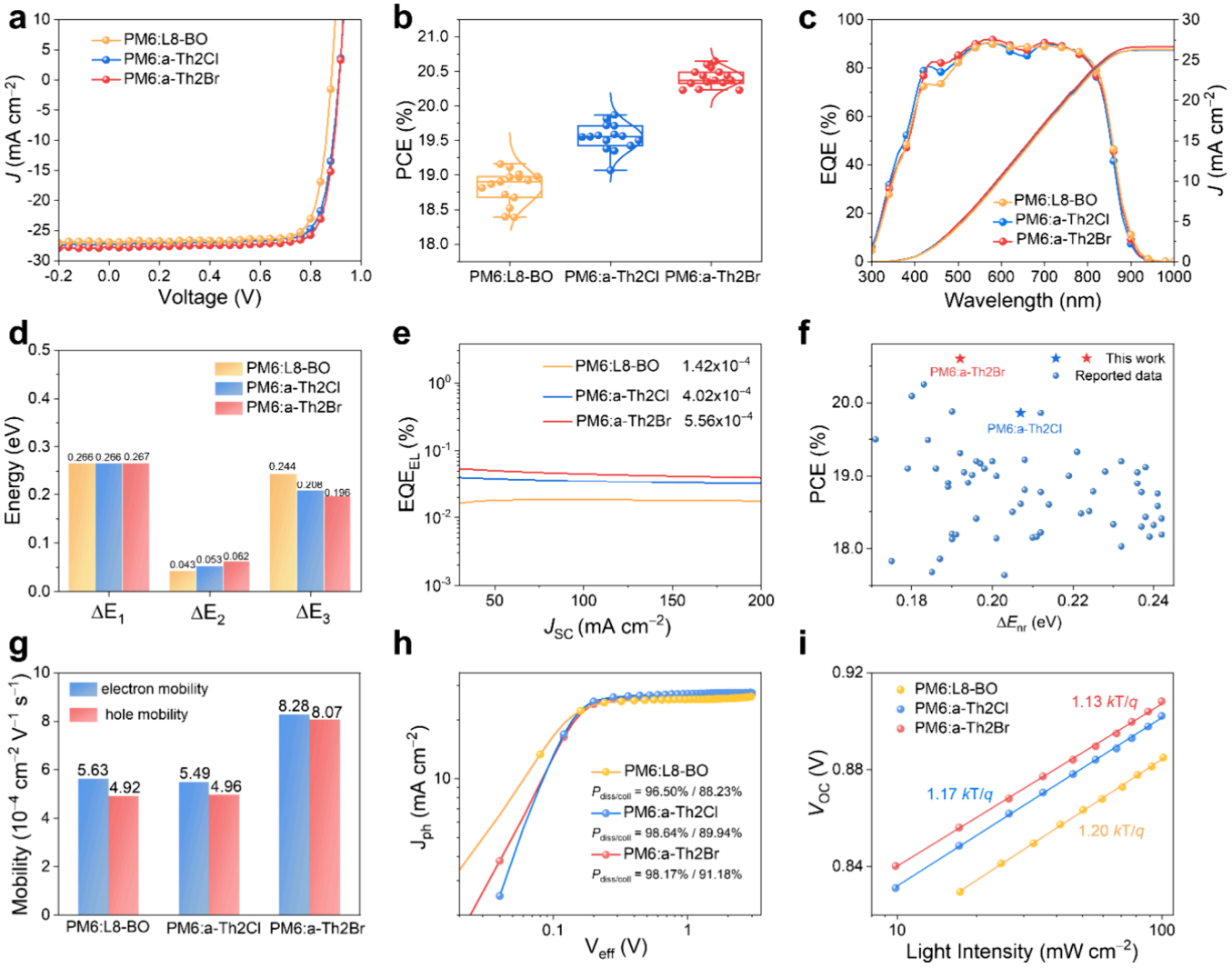

Figure 3. (a) $J-V$ curves. (b) Efficiency-distributed histograms of the three devices. (c) EQE responses. (d) Summary of detailed energy losses terms of optimal devices. (e) EQE_{EL} patterns of the corresponding devices. (f) Plots of the PCE versus nonradiative energy losses for different systems. (g) Histograms of the hole and electron mobility of blended films. (h) The J_{ph} versus V_{eff} curves. (i) V_{OC} versus light intensity of PM6:L8-BO, PM6:a-Th2Cl, and PM6:a-Th2Br devices.

Th2Cl, and a-Th2Br are 76.18, 57.29, and 53.38% (Figure 2e), respectively, clearly showing that this asymmetric molecule significantly suppresses the ACQ effect and will contribute to decrease ΔE_{nr} in relevant OSCs according to the established results on the energy losses mechanism analysis.[6]

The τ values for L8-BO, a-Th2Cl, and a-Th2Br are 1.24, 1.37, and 1.40 ns (Figure S8), respectively. Based on the equation of PLQY $= \frac{k_r}{k_r + k_{nr}} = \tau k_r$,[11,39,40] the radiative (k_r) and nonradiative (k_{nr}) recombination rate constants are 3.55×10^7 and 7.71×10^8, 6.22×10^7 and 6.68×10^8, and 6.89×10^7 and 6.45×10^8 s^{-1} for L8-BO, a-Th2Cl, and a-Th2Br, respectively. The fast radiative decay process and high PLQY are observed in a-Th2Cl and a-Th2Br, which should be attributed to their twisted central core units and efficient J-aggregation. According to the Marcus–Levich–Jortner theory, k_{nr} can be described by the equation:[41,42]

$$k_{nr} = V^2(4\pi\lambda_s k_B T)^{-0.5} \sum_{j=0}^{\infty} \frac{e^{-s} s^j}{j^i} \exp\left[-\frac{(E_{CT} - jh\bar{\upsilon} - \lambda_s)^2}{4\pi\lambda_s k_B T}\right]$$

here, $\bar{\upsilon}$ is the mean frequency of high-frequency vibrations, and other parameters are described in the Supporting Information. Enhancing molecular rigidity or lattice ordering can effectively inhibit vibrations, thus minimizing electron–phonon coupling and curtailing nonradiative energy losses in OSCs.[43] Therefore, we measured the temperature-dependent steady-state photoluminescence (PL) spectra (excited at 765 nm) for L8-BO, a-Th2Cl, and a-Th2Br, which have been shown in Figure S10. The electron–phonon coupling strength (γ_{LO}) of these acceptors was calculated by fitting the temperature-dependent fwhm of the PL peaks, $\Gamma(T)$, using the following equation: $\Gamma(T) = \Gamma_0 + \Gamma_{LO} = \Gamma_0 + \frac{\gamma_{LO}}{e^{\frac{E_{LO}}{k_B T}} - 1}$, where Γ_0 represents a temperature-independent constant due to scattering from structural disorder or imperfections, Γ_{LO} accounts for the longitudinal optical (LO) phonon (Fröhlich) interaction, γ_{LO} is the coupling strength, and E_{LO} is the LO phonon energy.[43] The calculated Γ_0 values were 66 meV for L8-BO, 54 meV for a-Th2Cl, and 52 meV for a-Th2Br (Figure 2f), which suggest enhanced structural ordering. The γ_{LO} values were determined to be 1.03, 0.75, and 0.58 eV for L8-BO, a-Th2Cl, and a-

https://doi.org/10.1021/jacs.5c13302
J. Am. Chem. Soc. 2025, 147, 43629–43639

Table 1. Photovoltaic Performance Parameters of OSCs Based on PM6:L8-BO, PM6:a-Th2Cl, and PM6:a-Th2Br and Measured under the Illumination of AM 1.5G (100 mW cm^{-2})

active layer	V_{OC} [V]	J_{SC} [mA cm^{-2}]	J_{SC}^{cal}[a] [mA cm^{-2}]	FF [%]	PCE[b] [%]
PM6:L8-BO	0.882 (0.881 ± 0.003)	26.90 (26.65 ± 0.35)	26.33	80.77 (80.22 ± 0.69)	19.16 (18.83 + 0.23)
PM6:a-Th2Cl	0.913 (0.911 ± 0.002)	27.12 (26.75 ± 0.30)	26.25	80.25 (80.17 ± 0.48)	19.87 (19.55 ± 0.20)
PM6:a-Th2Br	0.914 (0.915 ± 0.001)	27.67 (27.68 ± 0.19)	26.64	81.47 (80.56 ± 0.63)	20.60 (20.41 ± 0.13)
PM6:a-Th2Br[c]	0.920	26.64		81.81	20.05

[a]The J_{SC}^{cal} is determined from integration of the EQEs to the AM1.5G spectrum. [b]The values in parentheses are average parameters obtained from 15 devices. [c]Certified values in the Tianjin Institute of Metrological Supervision and Testing Electronic & Instrumental Laboratory.

Table 2. Detailed Energy Loss of the OSCs Based on the PM6:Acceptor Blend

active layer	V_{OC} (V)	E_g[a] (eV)	V_{oc}^{SQ}[b] (V)	ΔE_1 (eV)	ΔE_2 (eV)	ΔE_3 (eV)	EQE_{EL} (10^{-4})	ΔE_3[c] (eV)	E_{loss} (eV)
PM6:L8-BO	0.882	1.435	1.169	0.266	0.043	0.244	1.42	0.229	0.553
PM6:a-Th2Cl	0.913	1.440	1.173	0.266	0.053	0.208	4.02	0.202	0.527
PM6:a-Th2Br	0.914	1.439	1.172	0.267	0.062	0.196	5.56	0.194	0.525

[a]E_g is estimated by the derivatives of the EQE spectra (dEQE/dE). [b]V_{oc}^{SQ} is the maximum V_{OC} by the Shockley−Queisser (SQ) limit. [c]ΔE_3 represents the nonradiative recombination loss, which is calculated from EQE_{EL} using the equation $\Delta E_3 = -(k_B T/q)\ln EQE_{EL}$. Here, k is the Boltzmann constant and T is the temperature.

Th2Br, respectively (Figure 2f), reflecting effective suppression of electron−phonon coupling. As discussed above, in the crystal structure, a-Th2Br adopts a curved backbone, in which the thiophene unit is connected to the central pyrazine unit through a single bond, leading to a twisted conformation with a dihedral angle of around 9°. In contrast, the L8-BO molecule displays a planar backbone. Grazing incidence wide-angle X-ray scattering (GIWAXS) measurements of neat films reveal that a-Th2Br exhibits a longer crystal coherence length (CCL) than L8-BO (Table S4). These findings indicate that the twisted conformation between the grafted thiophene unit and the molecular backbone can enhance structural ordering, thereby reducing electron−phonon coupling and minimizing the ΔE_{nr} in OSC devices.

To further understand excited-state characteristics of molecular aggregates in films and their impact on k_r values, we carried out all-atom molecular dynamics (MD) simulations on L8-BO and a-Th2Br films and then performed time-dependent density functional theory (TDDFT) calculations on their 1000 dimers extracted from our MD-simulated films (for details, see "Computational Methods" section in the Supporting Information). Via our MD-TDDFT calculation, we examined the percentage of charge-transfer (CT) character and fluorescent oscillator strength (f_{osc}) for the S_1 states of L8-BO and a-Th2Br dimers, the values averaged on the 1000 dimers. Our MD-TDDFT calculation results revealed that the a-Th2Br aggregates exhibit a lower percentage of CT (84.82%) compared to the L8-BO aggregates (90.01%), which could result from a longer $\pi-\pi$ intermolecular distance for a-Th2Br aggregates. This is consistent with the distance trend observed by grazing incidence wide-angle X-ray scattering (GIWAXS) for L8-BO and a-Th2Br neat films (Table S4). When we analyzed the different packing patterns in terms of the percentage of CT and f, we found that the trends observed for the individual molecules held true across the packing configurations (Table S3). With an enhancement in the CT characteristic of the S_1 excited states, f_{osc} is normally reduced. Indeed, our calculation results indicated that a-Th2Br displays a larger f_{osc} of 0.30, as opposed to the value of 0.24 for L8-BO (Figure 2g). According to the rate formula of spontaneous emission, $k_r \propto f_{osc}$. As a result of the larger f_{osc} value for the a-Th2Br aggregates in the film, its k_r value is thus larger as shown in the above experimental results. This enhancement in k_r contributes to a higher PLQY for a-Th2Br compared to that for L8-BO as discussed above.

To evaluate the photovoltaic properties of the two acceptors, OSC devices were fabricated with a conventional architecture of ITO/2PACZ/active layer/F3N/Ag. For comparison, a control device based on L8-BO was also fabricated by using the same device structure and donor material PM6. Details of the device fabrication processes are provided in the Supporting Information. The optimized current density−voltage ($J-V$) curves are shown in Figure 3a, and the related device parameters are summarized in Table 1. The PM6:L8-BO- and PM6:a-Th2Cl-based devices exhibited PCEs of 19.16 and 19.87%, with V_{OC} values of 0.882 and 0.913 V, respectively. More excitingly, a comprehensive enhancement of photovoltaic parameters was observed in the PM6:a-Th2Br-based device, achieving a high PCE of 20.60% (certified 20.05%), with a high V_{OC} of 0.914 V, J_{SC} of 27.67 mA cm^{-2}, and FF of 81.47%. Notably, the PCE of 20.60% ranks among the few reported binary OSCs that have surpassed the 20% efficiency threshold. The external quantum efficiency (EQE) spectra of the devices are displayed in Figure 3c. The integrated J_{SC} values from the EQE curves were calculated to be 26.33, 26.25, and 26.64 mA cm^{-2} for PM6:L8-BO-, PM6:a-Th2Cl-, and PM6:a-Th2Br-based OSCs, which are in agreement with the measured J_{SC} values in the $J-V$ curves. Additionally, the initial stability of the three devices was evaluated under identical conditions. Devices based on PM6:a-Th2Cl and PM6:a-Th2Br exhibited slightly higher stability than those based on PM6:L8-BO. As shown in Figure S13, the a-Th2Cl- and a-Th2Br-based devices retained over 93% of their initial PCE after 700 h of room-temperature storage, approximately 87% after 700 h of thermal aging at 65 °C and around 80% after 300 h under maximum power point (MPP) tracking. In comparison, the PM6:L8-BO-based device maintained 91.6, 80.4, and 76.2% of its initial PCE under the same storage, thermal, and MPP stability tests, respectively.

To gain insight into the high V_{OC} obtained in both systems, the energy losses (E_{loss}) in all devices have been analyzed (Figure 3d), and the relevant data are summarized in Table 2. According to the Shockley−Queisser (SQ) limit theory, the energy losses (E_{loss}) of OSCs can be divided into three

https://doi.org/10.1021/jacs.5c13302
J. Am. Chem. Soc. 2025, 147, 43629−43639

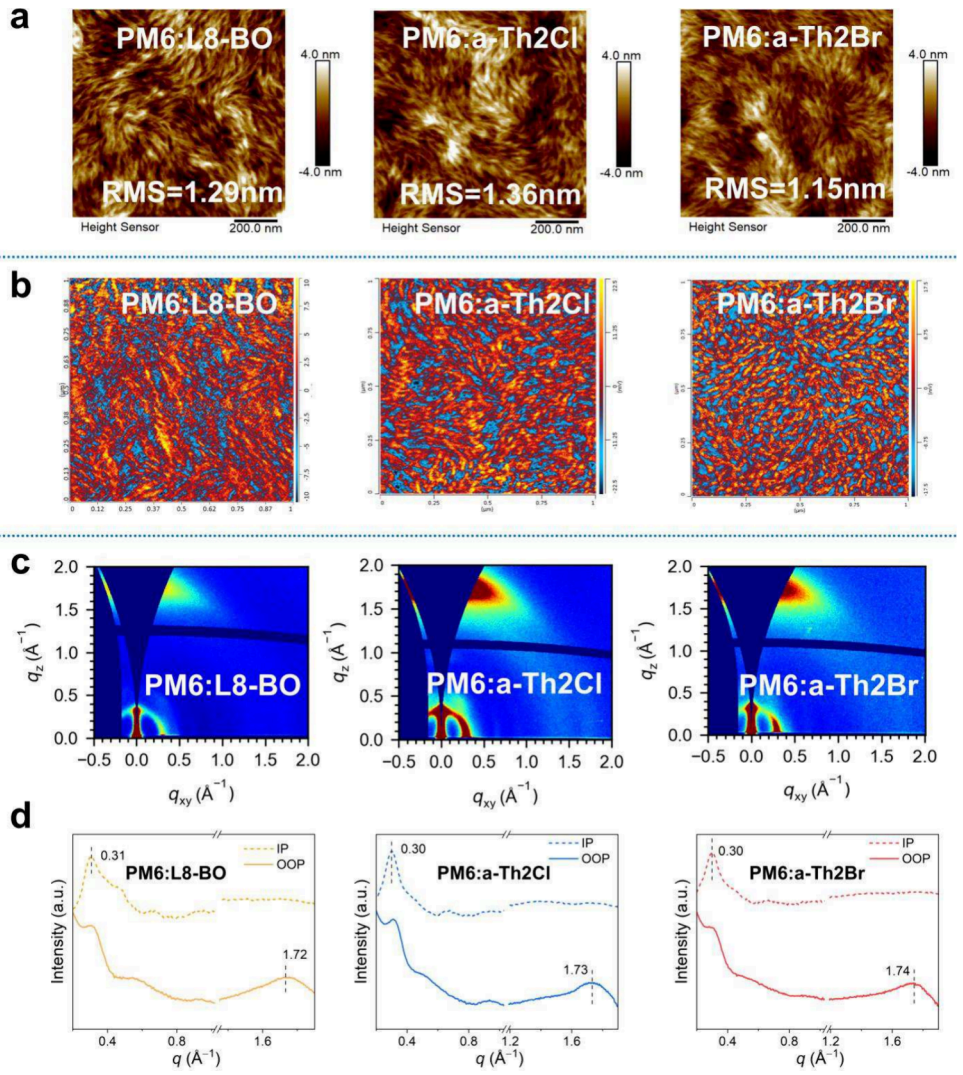

Figure 4. (a) AFM height images. (b) AFM-IR phase images of three blended films by measuring 2216 cm^{-1} signal of acceptors, in which donor and acceptor domains were marked with blue and red colors, respectively. (c) 2D GIWAXS patterns. (d) Corresponding 1D line-cuts of PM6:L8-BO, PM6:a-Th2Cl, and PM6:a-Th2Br blend films.

components, as described by the equation $E_{loss} = \Delta E_1 + \Delta E_2 + \Delta E_3$. The first component ΔE_1 is defined as $E_g - V_{OC}^{SQ}$, which is unavoidable for all types of solar cells originating from the radiative energy losses above the band gap. The E_g values of the L8-BO, a-Th2Cl, and a-Th2Br blends were 1.435, 1.439, and 1.440 eV, respectively, determined by differentiating the EQE spectra (dEQE/dE) (Figure S14). The total energy losses of L8-BO-, a-Th2Cl-, and a-Th2Br-based devices are 0.553, 0.527, and 0.525 eV, respectively, following the equation $E_{loss} = E_g - qV_{OC}$. There is no significant difference in terms of ΔE_1 due to the similar energy gaps of the three acceptor-based devices. The ΔE_2 refers to the radiative recombination losses below the bandgap and is attributed to nonstep function absorption and can be calculated from qV_{OC}^{SQ}-V_{OC}^{rad}. The ΔE_2 values of the L8-BO-, a-Th2Cl-, and a-Th2Br-based devices are 0.043, 0.053, and 0.062 eV, respectively. The third component ΔE_3 is caused by nonradiative recombination, which can be directly obtained by measuring the electroluminescence quantum efficiency (EQE_{EL}) of the device. We then calculated the nonradiative energy losses following the equation $\Delta E_3 = -(k_BT/q)\ln EQE_{EL}$. From the EQE_{EL} plots (Figure 3e), the PM6:a-Th2Cl and PM6:a-Th2Br blends exhibit a high EQE_{EL} of 4.02 × 10^{-4} and 5.56 × 10^{-4}, resulting in a small ΔE_3 of 0.202 and 0.194 eV, respectively, which are lower than that of typical L8-BO-based device (0.229 eV), primarily due to the high PLQY of their blends as described in the previous section, representing one of the lowest ΔE_{nr} value reported so far (Figure 3f).

The charge transport, generation, and recombination measurements were conducted to reveal the reasons behind the different photovoltaic performances. First, the electron mobility (μ_e) and hole mobility (μ_h) of the three blend films were measured using the space-charge limited current (SCLC) measurements and the results are shown in Figure 3g. The (μ_e/μ_h) of the blend films of PM6:L8-BO, PM6:a-Th2Cl, and PM6:a-Th2Br were measured to be 5.63/4.92, 5.49/4.96, and 8.28/8.07 × 10^{-4} cm^2 V^{-1} s^{-1} corresponding to μ_e/μ_h ratios of 1.14, 1.11, and 1.03, respectively. Then, the exciton dissociation (P_{diss}) and charge collection efficiency (P_{coll}) were further evaluated by plots of the photocurrent density (J_{ph}) versus effective voltage (V_{eff}) (Figure 3h). Compared with that of 96.50%/88.23% for the L8-BO-based device, the values of P_{diss}/P_{coll} can be estimated as 98.64%/89.94% and

https://doi.org/10.1021/jacs.5c13302
J. Am. Chem. Soc. 2025, 147, 43629−43639

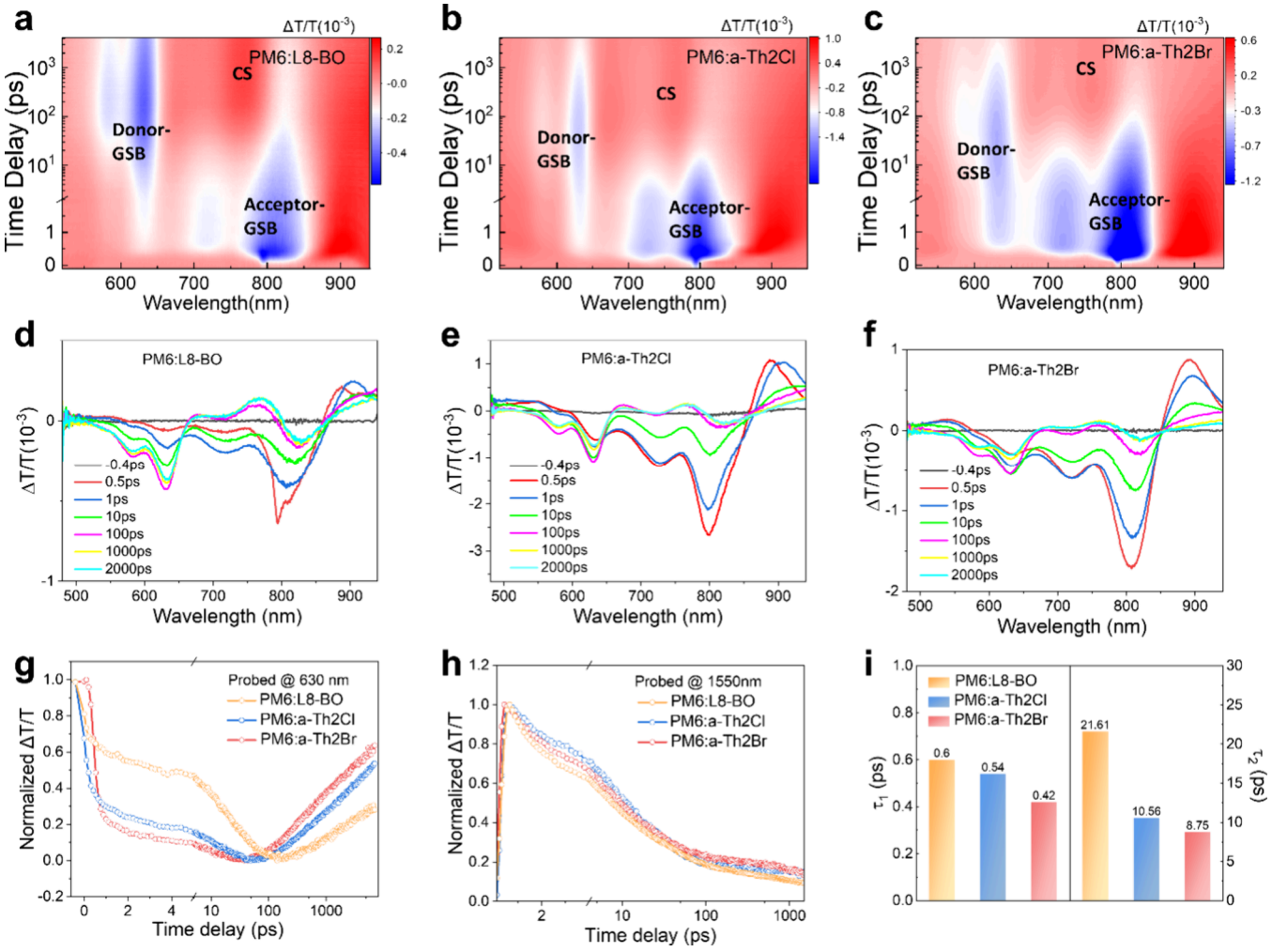

Figure 5. TA result of PM6:L8-BO, PM6:a-Th2Cl, and PM6:a-Th2Br blend films. (a–c) Contour plots of the time-resolved absorption difference spectra of the blend films under 800 nm excitation. (d–f) TA spectra of the blend films at different delay times. The hole transfer process at (g) 630 nm and (h) 1550 nm. (i) Statistical graphs of charge-transfer time and lifetime achieved through multiexponential fitting in corresponding conditions.

98.17%/91.18% for a-Th2Cl- and a-Th2Br-based devices, respectively. Subsequently, the charge recombination process was investigated through light-intensity (P_{light})-dependent V_{OC} and J_{SC} measurements. Focusing on the relationship of V_{OC} vs ln $P_{light}V_{OC} \propto kT/q$ ln(P_{light}), as illustrated in Figure 3i, the slopes for the L8-BO-, Th2Cl, and a-Th2Br-based devices are 1.20, 1.17, and 1.13 KT/q, respectively. All of the above results indicate that the devices based on the grafted core acceptor show superior charge dynamics, contributing to a higher J_{SC} and FF in binary devices.

The morphologies of the three blend films were systematically investigated using atomic force microscopy-based infrared spectroscopy (AFM-IR). As shown in the Figure 4a, a fibrillar network morphology was observed in the two blend films. Furthermore, all of the blend films possess a uniform and smooth surface. The values of root-mean-square (RMS) roughness of PM6:L8-BO, PM6:a-Th2Cl, and PM6:a-Th2Br are 1.29, 1.36, and 1.15 nm, respectively. Then, we recorded AFM-IR signals of blended films by detecting wavenumber at 2216 cm^{-1}, which is the stretching vibration of the C≡N bond in the three acceptors. As shown in the Figure 4b, it is obvious that interpenetrating fibrillary networks at nanoscale can be observed, especially for the PM6:a-Th2Br blend with a clearer D/A boundary, which are conducive to effective charge carrier transport, and thus enable the devices to achieve higher J_{SC} and FF. Based on a statistical analysis of nanofiber size in Figure S16, a reduced fiber size can be observed with 14.1 nm for PM6:a-Th2Cl and 14.7 nm for PM6:a-Th2Br, comparing to 18.3 nm for PM6:L8-BO, suggesting that the introduction of the grafted unit onto the central unit could enhance molecular crystallinity and fine-tune-phase domain sizes. Grazing incidence wide-angle X-ray scattering (GIWAXS) measurement was then performed to investigate the molecular ordering and packing behavior of the pristine and blend films. The scattering patterns in Figure 4c indicate the blend films also exhibit face-on orientation, similar to the neat films, which is found to be favorable for charge transport.[44] As summarized in Table S5, the (100) diffraction peaks in the in-plane (IP) direction for the L8-BO-, a-Th2Cl-, and a-Th2Br-blended films appear at 0.31, 0.30, and 0.30 $Å^{-1}$, corresponding to lamellar stacking distances of 20.26, 20.73, and 20.73 Å, respectively. In the out-of-plane (OOP) direction, prominent (010) peaks associated with $\pi-\pi$ stacking are observed at 1.72, 1.73, and 1.74 $Å^{-1}$ for the L8-BO-, a-Th2Cl-, and a-Th2Br-based blends, respectively. The corresponding $\pi-\pi$ stacking distances are 3.65, 3.63, and 3.65 Å, with CCLs of 21.25, 27.84, and 31.23 Å

https://doi.org/10.1021/jacs.5c13302
J. Am. Chem. Soc. 2025, 147, 43629–43639

(Figure 4d). These results indicate that although the *d*-spacing of pure a-Th2Cl and a-Th2Br films increases compared to L8-BO, they can still achieve tighter and more ordered packing when blended with the donor, which is conducive to improving exciton dissociation, charge transport, and collection, thereby significantly enhancing J_{SC} and FF, suppressing energy losses, and yielding high photovoltaic performance.

Apart from film morphology, the investigation of exciton and charge dynamics can give us a deeper understanding of the exciton transport and charge generation behavior in the active layer. Then, we studied the hole transfer dynamics of blend films through transient absorption spectroscopy (TAS) measurement. Due to the distinct absorption regions of the polymer donor and acceptor, we employed a low power pump light at 800 nm to exclusively excite the acceptor. As shown in Figure 5, a new GSB signal at 630 nm, representing PM6 absorption, showed up immediately, suggesting rapid hole transfer from the acceptor to the donor upon selective photoexcitation of acceptors. By fitting the GSB signals using a biexponential model, the τ_1 and τ_2 values were obtained, where τ_1 represents the dissociation time of exciton at the D:A interface and τ_2 represents the exciton diffusion time to the D:A interface.[45] Smaller fitted parameters (τ_1 and τ_2) of PM6:a-Th2Cl (τ_1 = 0.54 ± 0.01 ps, τ_2 = 10.56 ± 0.50 ps) and PM6:a-Th2Br (τ_1 = 0.42 ± 0.02 ps, τ_2 = 8.75 ± 1.48 ps) blend films (Figure 5g) indicate that exciton dissociation and diffusion are more efficient than those in PM6:L8-BO blend film (τ_1 = 0.60 ± 0.02 ps, τ_2 = 21.62 ± 0.36 ps), which is beneficial for suppressing charge recombination, thus improving J_{SC} and FF. The photoluminescence (PL) quenching measurements were carried out to study the charge-transfer efficiency (Figure S18). Both of the a-Th2Cl- and a-Th2Br-based blend films exhibit highly efficient electron transfer efficiency due to the sufficient driving force from the LUMO energy offset. When the acceptor was selected excited, the a-Th2Cl- and a-Th2Br-based blends display hole transfer efficiencies of 90.5 and 91.5%, respectively. Meanwhile, we also observed the i-Ex state, which exhibit low exciton binding energy with the electron and hole on separate molecules at around 1550 nm (Figure S17). The generation of i-Ex tends to facilitate the charge generation, which is evidenced by the formation of charge state (CS) at 750 nm in the acceptor phase of blends as earlier reported.[46] The i-Ex lifetimes in the PM6:L8-BO, PM6:a-Th2Cl, and PM6:a-Th2Br blend films are 18.55, 24.77, and 35.37 ps (Figure 5h), respectively. The longer i-Ex lifetime of PM6:a-Th2Br blends is consistent with the reduced nonradiative charge recombination, corresponding to the low ΔE_{nr}.[47]

CONCLUSIONS

In this study, we designed and synthesized two acceptors, a-Th2Cl and a-Th2Br, which feature a central core-twisted conformation. This was achieved by introducing chlorinated and brominated thiophene units onto the central pyrazine cores of the Y-series acceptors through single-bond linkages. Comprehensive analyses including crystallographic studies, molecular simulations, and photophysical properties revealed that this twisted core design effectively suppresses the undesirable aggregation-caused quenching (ACQ) effect while maintaining efficient intermolecular packing, thereby contributing to a reduced ΔE_{nr}. Although a-Th2Cl and a-Th2Br exhibit the same optical bandgap as L8-BO, they achieved lower ΔE_{nr} values of 0.202 and 0.194 eV, respectively, compared to L8-BO (0.229 eV). As a result, a high PCE of 20.60% was achieved with PM6:a-Th2Br, demonstrating a high V_{OC} of 0.914 V, J_{SC} of 27.67 mA cm^{-2}, and FF of 81.47%. This places it among the few reported binary OSCs to surpass the 20% efficiency threshold, owing to simultaneous enhancement of all three key performance parameters. These results highlight the distinct advantage and potential of the twisted central core conformation molecular design, particularly its influence on molecular packing, and may offer valuable guidance for the development of high-performance acceptors.

ASSOCIATED CONTENT

Supporting Information

The Supporting Information is available free of charge at https://pubs.acs.org/doi/10.1021/jacs.5c13302.

Materials and characterization methods, material synthesis, device fabrication and measurement, NMR spectra and mass spectra, UV−vis absorption, cyclic voltammetry, DFT calculations, space-charge-limited current measurement, temperature-dependent PL spectra measurement, light-intensity-dependent, transient photovoltage,and transient photocurrent measurements, energy losses and photovoltaic bandgap measurements, GIWAXS analysis, fs-TA spectroscopy, photovoltaic data, and references (PDF)

Accession Codes

Deposition Number 2463775 contains the supplementary crystallographic data for this paper. These data can be obtained free of charge via the joint Cambridge Crystallographic Data Centre (CCDC) and Fachinformationszentrum Karlsruhe Access Structures service.

AUTHOR INFORMATION

Corresponding Authors

Xian-Kai Chen − *Institute of Functional Nano & Soft Materials (FUNSOM), Joint International Research Laboratory of Carbon-Based Functional Materials and Devices, State Key Laboratory of Bioinspired interfacial Materials Science, Soochow University, Suzhou, Jiangsu 215123, P. R. China;* orcid.org/0000-0002-8580-7246; Email: xkchen@suda.edu.cn

Xiangjian Wan − *State Key Laboratory of Elemento-Organic Chemistry, Frontiers Science Center for New Organic Matter, The Centre of Nanoscale Science and Technology and Key Laboratory of Functional Polymer Materials, Institute of Polymer Chemistry, College of Chemistry, Renewable Energy Conversion and Storage Center (RECAST), Nankai University, Tianjin 300071, China;* orcid.org/0000-0001-5266-8510; Email: xjwan@nankai.edu.cn

Yongsheng Chen − *State Key Laboratory of Elemento-Organic Chemistry, Frontiers Science Center for New Organic Matter, The Centre of Nanoscale Science and Technology and Key Laboratory of Functional Polymer Materials, Institute of Polymer Chemistry, College of Chemistry, Renewable Energy Conversion and Storage Center (RECAST), Nankai University, Tianjin 300071, China;* orcid.org/0000-0003-1448-8177; Email: yschen99@nankai.edu.cn

Authors

Ruohan Wang − *State Key Laboratory of Elemento-Organic Chemistry, Frontiers Science Center for New Organic Matter, The Centre of Nanoscale Science and Technology and Key*

Laboratory of Functional Polymer Materials, Institute of Polymer Chemistry, College of Chemistry, Renewable Energy Conversion and Storage Center (RECAST), Nankai University, Tianjin 300071, China

Xiaodong Si − *State Key Laboratory of Elemento-Organic Chemistry, Frontiers Science Center for New Organic Matter, The Centre of Nanoscale Science and Technology and Key Laboratory of Functional Polymer Materials, Institute of Polymer Chemistry, College of Chemistry, Renewable Energy Conversion and Storage Center (RECAST), Nankai University, Tianjin 300071, China*

Le Mei − *Institute of Functional Nano & Soft Materials (FUNSOM), Joint International Research Laboratory of Carbon-Based Functional Materials and Devices, State Key Laboratory of Bioinspired interfacial Materials Science, Soochow University, Suzhou, Jiangsu 215123, P. R. China; Department of Chemistry, City University of Hong Kong, Hong Kong 999077, China*

Wenkai Zhao − *School of Materials Science and Engineering, National Institute for Advanced Materials, Renewable Energy Conversion and Storage Center (RECAST), Nankai University, Tianjin 300350, China*

Wendi Shi − *State Key Laboratory of Elemento-Organic Chemistry, Frontiers Science Center for New Organic Matter, The Centre of Nanoscale Science and Technology and Key Laboratory of Functional Polymer Materials, Institute of Polymer Chemistry, College of Chemistry, Renewable Energy Conversion and Storage Center (RECAST), Nankai University, Tianjin 300071, China*

Guangkun Song − *State Key Laboratory of Elemento-Organic Chemistry, Frontiers Science Center for New Organic Matter, The Centre of Nanoscale Science and Technology and Key Laboratory of Functional Polymer Materials, Institute of Polymer Chemistry, College of Chemistry, Renewable Energy Conversion and Storage Center (RECAST), Nankai University, Tianjin 300071, China*

Longyu Li − *State Key Laboratory of Elemento-Organic Chemistry, Frontiers Science Center for New Organic Matter, The Centre of Nanoscale Science and Technology and Key Laboratory of Functional Polymer Materials, Institute of Polymer Chemistry, College of Chemistry, Renewable Energy Conversion and Storage Center (RECAST), Nankai University, Tianjin 300071, China*

Zheng Xiao − *State Key Laboratory of Elemento-Organic Chemistry, Frontiers Science Center for New Organic Matter, The Centre of Nanoscale Science and Technology and Key Laboratory of Functional Polymer Materials, Institute of Polymer Chemistry, College of Chemistry, Renewable Energy Conversion and Storage Center (RECAST), Nankai University, Tianjin 300071, China*

Zhaoyang Yao − *State Key Laboratory of Elemento-Organic Chemistry, Frontiers Science Center for New Organic Matter, The Centre of Nanoscale Science and Technology and Key Laboratory of Functional Polymer Materials, Institute of Polymer Chemistry, College of Chemistry, Renewable Energy Conversion and Storage Center (RECAST), Nankai University, Tianjin 300071, China;* orcid.org/0000-0003-1384-183X

Guankui Long − *School of Materials Science and Engineering, National Institute for Advanced Materials, Renewable Energy Conversion and Storage Center (RECAST), Nankai University, Tianjin 300350, China;* orcid.org/0000-0002-1826-3736

Chenxi Li − *State Key Laboratory of Elemento-Organic Chemistry, Frontiers Science Center for New Organic Matter, The Centre of Nanoscale Science and Technology and Key Laboratory of Functional Polymer Materials, Institute of Polymer Chemistry, College of Chemistry, Renewable Energy Conversion and Storage Center (RECAST), Nankai University, Tianjin 300071, China*

Complete contact information is available at: https://pubs.acs.org/10.1021/jacs.5c13302

Author Contributions

[‡]R.W. and X.S. contributed equally to this work.

Notes

The authors declare no competing financial interest.

■ ACKNOWLEDGMENTS

The authors gratefully acknowledge the financial support from National Natural Science Foundation of China (52025033, 52373189, and 22361132530) and Ministry of Science and Technology of China (2022YFB4200400). X.-K.C. gratefully acknowledges the financial supports from the National Natural Science Foundation of China (grant no. 52473190), the Natural Science Foundation of Jiangsu Province (grant no. BK20240042), the Science and Technology Project of Suzhou (grant no. ZXL2024394), the Suzhou Key Laboratory of Functional Nano & Soft Materials, the Collaborative Innovation Center of Suzhou Nano Science & Technology, and the 111 Project.

■ REFERENCES

(1) Guan, S.; Li, Y.; Xu, C.; Yin, N.; Xu, C.; Wang, C.; Wang, M.; Xu, Y.; Chen, Q.; Wang, D.; Zuo, L.; Chen, H. Self-Assembled Interlayer Enables High-Performance Organic Photovoltaics with Power Conversion Efficiency Exceeding 20%. *Adv. Mater.* **2024**, *36* (25), 2400342.

(2) Zhu, L.; Zhang, M.; Zhou, G.; Wang, Z.; Zhong, W.; Zhuang, J.; Zhou, Z.; Gao, X.; Kan, L.; Hao, B.; Han, F.; Zeng, R.; Xue, X.; Xu, S.; Jing, H.; Xiao, B.; Zhu, H.; Zhang, Y.; Liu, F. Achieving 20.8% organic solar cells via additive-assisted layer-by-layer fabrication with bulk p-i-n structure and improved optical management. *Joule* **2024**, *8* (11), 3153−3168.

(3) Chen, C.; Wang, L.; Xia, W.; Qiu, K.; Guo, C.; Gan, Z.; Zhou, J.; Sun, Y.; Liu, D.; Li, W.; Wang, T. Molecular interaction induced dual fibrils towards organic solar cells with certified efficiency over 20%. *Nat. Commun.* **2024**, *15* (1), 6865.

(4) Jiang, Y.; Sun, S.; Xu, R.; Liu, F.; Miao, X.; Ran, G.; Liu, K.; Yi, Y.; Zhang, W.; Zhu, X. Non-fullerene acceptor with asymmetric structure and phenyl-substituted alkyl side chain for 20.2% efficiency organic solar cells. *Nat. Energy* **2024**, *9* (8), 975−986.

(5) Chen, H.; Huang, Y.; Zhang, R.; Mou, H.; Ding, J.; Zhou, J.; Wang, Z.; Li, H.; Chen, W.; Zhu, J.; Cheng, Q.; Gu, H.; Wu, X.; Zhang, T.; Wang, Y.; Zhu, H.; Xie, Z.; Gao, F.; Li, Y.; Li, Y. Organic solar cells with 20.82% efficiency and high tolerance of active layer thickness through crystallization sequence manipulation. *Nat. Mater.* **2025**, *24* (3), 444−453.

(6) Li, C.; Song, J.; Lai, H.; Zhang, H.; Zhou, R.; Xu, J.; Huang, H.; Liu, L.; Gao, J.; Li, Y.; Jee, M. H.; Zheng, Z.; Liu, S.; Yan, J.; Chen, X.-K.; Tang, Z.; Zhang, C.; Woo, H. Y.; He, F.; Gao, F.; Yan, H.; Sun, Y. Non-fullerene acceptors with high crystallinity and photoluminescence quantum yield enable 20% efficiency organic solar cells. *Nat. Mater.* **2025**, *24* (3), 433−443.

(7) Li, C.; Yao, G.; Gu, X.; Lv, J.; Hou, Y.; Lin, Q.; Yu, N.; Abbasi, M. S.; Zhang, X.; Zhang, J.; Tang, Z.; Peng, Q.; Zhang, C.; Cai, Y.; Huang, H. Highly efficient organic solar cells enabled by suppressing

triplet exciton formation and non-radiative recombination. *Nat. Commun.* **2024**, *15* (1), 8872.
(8) Xie, Y.; Tian, J.; Yang, X.; Chen, J.; Yu, S.; Tang, D.; Hu, X.; Sun, Y.; Lv, M. Thiophene Expanded Self-Assembled Monolayer as Hole Transport Layer for Organic Solar Cells with Efficiency of 20.78%. *Adv. Mater.* **2025**, No. e02485.
(9) Li, C.; Cai, Y.; Hu, P.; Liu, T.; Zhu, L.; Zeng, R.; Han, F.; Zhang, M.; Zhang, M.; Lv, J.; Ma, Y.; Han, D.; Zhang, M.; Lin, Q.; Xu, J.; Yu, N.; Qiao, J.; Wang, J.; Zhang, X.; Xia, J.; Tang, Z.; Ye, L.; Li, X.; Xu, Z.; Hao, X.; Peng, Q.; Liu, F.; Guo, L.; Huang, H. Organic solar cells with 21% efficiency enabled by a hybrid interfacial layer with dual-component synergy. *Nat. Mater.* **2025**, *24*, 1626.
(10) Liu, S.; Yuan, J.; Deng, W.; Luo, M.; Xie, Y.; Liang, Q.; Zou, Y.; He, Z.; Wu, H.; Cao, Y. High-efficiency organic solar cells with low non-radiative recombination loss and low energetic disorder. *Nat. Photonics* **2020**, *14* (5), 300−305.
(11) Kong, Y.; Chen, H.; Zuo, L. Understanding the Nonradiative Charge Recombination in Organic Photovoltaics: From Molecule to Device. *Adv. Funct. Mater.* **2024**, *35* (3), 2413864.
(12) Gillett, A. J.; Privitera, A.; Dilmurat, R.; Karki, A.; Qian, D.; Pershin, A.; Londi, G.; Myers, W. K.; Lee, J.; Yuan, J.; Ko, S.-J.; Riede, M. K.; Gao, F.; Bazan, G. C.; Rao, A.; Nguyen, T.-Q.; Beljonne, D.; Friend, R. H. The role of charge recombination to triplet excitons in organic solar cells. *Nature* **2021**, *597* (7878), 666−671.
(13) Rao, A.; Chow, P. C. Y.; Gélinas, S.; Schlenker, C. W.; Li, C.-Z.; Yip, H.-L.; Jen, A. K. Y.; Ginger, D. S.; Friend, R. H. The role of spin in the kinetic control of recombination in organic photovoltaics. *Nature* **2013**, *500* (7463), 435−439.
(14) Qian, D.; Zheng, Z.; Yao, H.; Tress, W.; Hopper, T. R.; Chen, S.; Li, S.; Liu, J.; Chen, S.; Zhang, J.; Liu, X.-K.; Gao, B.; Ouyang, L.; Jin, Y.; Pozina, G.; Buyanova, I. A.; Chen, W. M.; Inganäs, O.; Coropceanu, V.; Bredas, J.-L.; Yan, H.; Hou, J.; Zhang, F.; Bakulin, A. A.; Gao, F. Design rules for minimizing voltage losses in high-efficiency organic solar cells. *Nat. Mater.* **2018**, *17* (8), 703−709.
(15) Liu, Y.; Liu, B.; Ma, C.-Q.; Huang, F.; Feng, G.; Chen, H.; Hou, J.; Yan, L.; Wei, Q.; Luo, Q.; Bao, Q.; Ma, W.; Liu, W.; Li, W.; Wan, X.; Hu, X.; Han, Y.; Li, Y.; Zhou, Y.; Zou, Y.; Chen, Y.; Li, Y.; Chen, Y.; Tang, Z.; Hu, Z.; Zhang, Z.-G.; Bo, Z. Recent progress in organic solar cells (Part I material science). *Sci. China Chem.* **2022**, *65* (2), 224−268.
(16) Yuan, J.; Zhang, Y.; Zhou, L.; Zhang, G.; Yip, H.-L.; Lau, T.-K.; Lu, X.; Zhu, C.; Peng, H.; Johnson, P. A.; Leclerc, M.; Cao, Y.; Ulanski, J.; Li, Y.; Zou, Y. Single-Junction Organic Solar Cell with over 15% Efficiency Using Fused-Ring Acceptor with Electron-Deficient Core. *Joule* **2019**, *3* (4), 1140−1151.
(17) Cui, Y.; Yao, H.; Zhang, J.; Xian, K.; Zhang, T.; Hong, L.; Wang, Y.; Xu, Y.; Ma, K.; An, C.; He, C.; Wei, Z.; Gao, F.; Hou, J. Single-Junction Organic Photovoltaic Cells with Approaching 18% Efficiency. *Adv. Mater.* **2020**, *32* (19), No. e1908205.
(18) Li, C.; Zhou, J.; Song, J.; Xu, J.; Zhang, H.; Zhang, X.; Guo, J.; Zhu, L.; Wei, D.; Han, G.; Min, J.; Zhang, Y.; Xie, Z.; Yi, Y.; Yan, H.; Gao, F.; Liu, F.; Sun, Y. Non-fullerene acceptors with branched side chains and improved molecular packing to exceed 18% efficiency in organic solar cells. *Nat. Energy* **2021**, *6* (6), 605−613.
(19) Li, Y.; Fu, H.; Wu, Z.; Wu, X.; Wang, M.; Qin, H.; Lin, F.; Woo, H. Y.; Jen, A. K. Y. Regulating the Aggregation of Unfused Non-Fullerene Acceptors via Molecular Engineering towards Efficient Polymer Solar Cells. *ChemSusChem* **2021**, *14* (17), 3579−3589.
(20) Lai, H.; Zhao, Q.; Chen, Z.; Chen, H.; Chao, P.; Zhu, Y.; Lang, Y.; Zhen, N.; Mo, D.; Zhang, Y.; He, F. Trifluoromethylation Enables a 3D Interpenetrated Low-Band-Gap Acceptor for Efficient Organic Solar Cells. *Joule* **2020**, *4* (3), 688−700.
(21) Li, W.; Chen, M.; Cai, J.; Spooner, E. L. K.; Zhang, H.; Gurney, R. S.; Liu, D.; Xiao, Z.; Lidzey, D. G.; Ding, L.; Wang, T. Molecular Order Control of Non-fullerene Acceptors for High-Efficiency Polymer Solar Cells. *Joule* **2019**, *3* (3), 819−833.
(22) Oh, J. M.; Venters, C. C.; Di, C.; Pinto, A. M.; Wan, L.; Younis, I.; Cai, Z.; Arai, C.; So, B. R.; Duan, J.; Dreyfuss, G. U1 snRNP regulates cancer cell migration and invasion in vitro. *Nat. Commun.* **2020**, *11* (1), 1.
(23) Zhang, H.; Zhao, Z.; Turley, A. T.; Wang, L.; McGonigal, P. R.; Tu, Y.; Li, Y.; Wang, Z.; Kwok, R. T. K.; Lam, J. W. Y.; Tang, B. Z. Aggregate Science: From Structures to Properties. *Adv. Mater.* **2020**, *32* (36), 2001457.
(24) Witte, F.; Rietsch, P.; Sinha, S.; Krappe, A.; Joswig, J.-O.; Götze, J. P.; Nirmalananthan-Budau, N.; Resch-Genger, U.; Eigler, S.; Paulus, B. Fluorescence Quenching in J-Aggregates through the Formation of Unusual Metastable Dimers. *J. Phys. Chem. B* **2021**, *125* (17), 4438−4446.
(25) Liu, Y.; Guo, Y.; Liu, Y. High-Mobility Organic Light-Emitting Semiconductors and Its Optoelectronic Devices. *Small Struct.* **2020**, *2* (1), 2000083.
(26) Lu, H.; Li, D.; Liu, W.; Ran, G.; Wu, H.; Wei, N.; Tang, Z.; Liu, Y.; Zhang, W.; Bo, Z. Designing A-D−A Type Fused-Ring Electron Acceptors with a Bulky 3D Substituent at the Central Donor Core to Minimize Non-Radiative Losses and Enhance Organic Solar Cell Efficiency. *Angew. Chem., Int. Ed.* **2024**, *63* (33), No. e202407007.
(27) Zhu, X.; Gu, C.; Cheng, Y.; Lu, H.; Wang, X.; Ran, G.; Zhang, W.; Tang, Z.; Bo, Z.; Liu, Y. 3D-Architectured Acceptor with High Photoluminescence Quantum Yield and Moderate Crystallinity for High-efficiency Organic Solar Cells with Low Voltage Loss. *Adv. Mater.* **2025**, *37* (35), 2507529.
(28) Wei, N.; Guo, Y.; Song, H.; Liu, Y.; Lu, H.; Bo, Z. Reducing Non-Radiative Energy Losses in Non-Fullerene Organic Solar Cells. *ChemSusChem* **2024**, *18* (6), No. e202402169.
(29) Song, G.; He, T.; Wang, R.; Ouyang, Y.; Jain, N.; Liu, S.; Kan, B.; Shang, Y.; Li, J.; Wang, X.; Yao, Z.; Wan, X.; Li, C.; Ma, W.; Zhao, Y.; Long, G.; Zhang, C.; Gao, F.; Chen, Y. Regulate the Singlet-Triplet Energy Gap by Spatially Separating HOMO and LUMO for High Performance Organic Photovoltaic Acceptors. *Angew. Chem., Int. Ed.* **2025**, *64* (35), No. e202506357.
(30) Yao, Z.; Wan, X.; Li, C.; Chen, Y. Two-Dimensional Conjugation Extended CH-Series Acceptors with a Distinctive A-D−A Character. *Accounts of Materials Research* **2023**, *4* (9), 772−785.
(31) Xie, M.; Wei, Z.; Lu, K. Quinoxaline-based Y-type acceptors for organic solar cells. *Chemical Science* **2024**, *15* (22), 8265−8279.
(32) Chen, H.; Zou, Y.; Liang, H.; He, T.; Xu, X.; Zhang, Y.; Ma, Z.; Wang, J.; Zhang, M.; Li, Q.; Li, C.; Long, G.; Wan, X.; Yao, Z.; Chen, Y. Lowing the energy loss of organic solar cells by molecular packing engineering via multiple molecular conjugation extension. *Sci. China Chem.* **2022**, *65* (7), 1362−1373.
(33) Li, C.; Fu, H.; Xia, T.; Sun, Y. Asymmetric Nonfullerene Small Molecule Acceptors for Organic Solar Cells. *Adv. Energy. Mater.* **2019**, *9* (25), 1900999.
(34) Gao, W.; Zhang, M.; Liu, T.; Ming, R.; An, Q.; Wu, K.; Xie, D.; Luo, Z.; Zhong, C.; Liu, F.; Zhang, F.; Yan, H.; Yang, C. Asymmetrical Ladder-Type Donor-Induced Polar Small Molecule Acceptor to Promote Fill Factors Approaching 77% for High-Performance Nonfullerene Polymer Solar Cells. *Adv. Mater.* **2018**, *30* (26), No. e1800052.
(35) Qiu, D.; Zhang, L.; Zhang, H.; Tang, A.; Zhang, J.; Wei, Z.; Lu, K. Elucidating the effects of bromine substitution in asymmetric quinoxaline central core-based non-fullerene acceptors on molecular stacking and photovoltaic performances. *J. Mater. Chem. A* **2025**, *13* (6), 4237−4246.
(36) He, H.; Li, X.; Zhang, J.; Chen, Z.; Gong, Y.; Zhuo, H.; Wu, X.; Li, Y.; Wang, S.; Bi, Z.; Song, B.; Zhou, K.; Liang, T.; Ma, W.; Lu, G.; Ye, L.; Meng, L.; Zhang, B.; Li, Y.; Li, Y. Dynamic hydrogen-bonding enables high-performance and mechanically robust organic solar cells processed with non-halogenated solvent. *Nat. Commun.* **2025**, *16* (1), 787.
(37) Zhang, Y.; Ji, Y.; Zhang, Y.; Zhang, W.; Bai, H.; Du, M.; Wu, H.; Guo, Q.; Zhou, E. Recent Progress of Y6-Derived Asymmetric Fused Ring Electron Acceptors. *Adv. Funct. Mater.* **2022**, *32* (35), 2205115.

(38) Ma, S.; Du, S.; Pan, G.; Dai, S.; Xu, B.; Tian, W. Organic molecular aggregates: From aggregation structure to emission property. *Aggregate* **2021**, *2* (4), No. e96.
(39) Jiang, Y.; Li, Y.; Liu, F.; Wang, W.; Su, W.; Liu, W.; Liu, S.; Zhang, W.; Hou, J.; Xu, S.; Yi, Y.; Zhu, X. Suppressing electron-phonon coupling in organic photovoltaics for high-efficiency power conversion. *Nat. Commun.* **2023**, *14* (1), 5079.
(40) Zuo, L.; Jo, S. B.; Li, Y.; Meng, Y.; Stoddard, R. J.; Liu, Y.; Lin, F.; Shi, X.; Liu, F.; Hillhouse, H. W.; Ginger, D. S.; Chen, H.; Jen, A. K. Dilution effect for highly efficient multiple-component organic solar cells. *Nat. Nanotechnol* **2022**, *17*, 53−60.
(41) Gould, I. R.; Noukakis, D.; Gomez-Jahn, L.; Young, R. H.; Goodman, J. L.; Farid, S. Radiative and nonradiative electron transfer in contact radical-ion pairs. *Chem. Phys.* **1993**, *176* (2), 439−456.
(42) Deibel, C.; Strobel, T.; Dyakonov, V. Role of the Charge Transfer State in Organic Donor-Acceptor Solar Cells. *Adv. Mater.* **2010**, *22* (37), 4097−4111.
(43) Yang, F.; Fang, H.; Guo, E.; Xiao, C.; Lu, Z.; Wang, Y.; Fan, H.; Zhang, A.; Lai, W.; Li, W. Oligomerized Electron Acceptors with Alkynyl Linkages to Suppress Electron-Phonon Coupling for Low-Energy-Loss Organic Solar Cells. *Angew. Chem., Int. Ed.* **2025**, *64* (15), No. e202501302.
(44) Wang, L.; Chen, C.; Fu, Y.; Guo, C.; Li, D.; Cheng, J.; Sun, W.; Gan, Z.; Sun, Y.; Zhou, B.; Liu, C.; Liu, D.; Li, W.; Wang, T. Donor−acceptor mutually diluted heterojunctions for layer-by-layer fabrication of high-performance organic solar cells. *Nat. Energy* **2024**, *9* (2), 208−218.
(45) Song, X.; Zhang, B.; Liu, X.; Mei, L.; Li, H.; Yin, S.; Zhou, X.; Chen, H.; Lin, Y.; Zhu, W.; Chen, X. Low-Volatility Fused-Ring Solid Additive Engineering for Synergistically Elongating Exciton Lifetime and Mitigating Trap Density Toward Organic Solar Cells of 20.5% Efficiency. *Adv. Mater.* **2025**, *37* (12), 2418393.
(46) Wang, R.; Zhang, C.; Li, Q.; Zhang, Z.; Wang, X.; Xiao, M. Charge Separation from an Intra-Moiety Intermediate State in the High-Performance PM6:Y6 Organic Photovoltaic Blend. *J. Am. Chem. Soc.* **2020**, *142* (29), 12751−12759.
(47) Huang, J.; Chen, T.; Mei, L.; Wang, M.; Zhu, Y.; Cui, J.; Ouyang, Y.; Pan, Y.; Bi, Z.; Ma, W.; Ma, Z.; Zhu, H.; Zhang, C.; Chen, X. K.; Chen, H.; Zuo, L. On the role of asymmetric molecular geometry in high-performance organic solar cells. *Nat. Commun.* **2024**, *15* (1), 3287.

https://doi.org/10.1021/jacs.5c13302
J. Am. Chem. Soc. 2025, 147, 43629−43639